

Bacterial Leaf Blight Detection in Rice Crops Using Ground-Based Spectroradiometer Data and Multi-temporal Satellites Images

Rani Yudarwati¹, Chiharu Hongo², Gunardi Sigit³, Baba Barus⁴ & Budi Utoyo³

¹ Graduate School of Science and Engineering, Chiba University, Japan

² Center for Environmental Remote Sensing, Chiba University, Japan

³ West Java Food Crops and Horticultural Agency, Indonesia

⁴ Bogor Agricultural University, Indonesia

Correspondence: Rani Yudarwati, Graduate School of Science and Engineering, Chiba University, Japan. Tel: 81-90-2535-0388. E-mail: rani.yudarwati@gmail.com

Received: October 29, 2019

Accepted: December 2, 2019

Online Published: January 15, 2020

doi:10.5539/jas.v12n2p38

URL: <https://doi.org/10.5539/jas.v12n2p38>

This research is supported by the Science and Technology Research Partnership for Sustainable Development (SATREPS).

Abstract

This study presents a method for detecting rice crop damage due to bacterial leaf blight (BLB) infestation. Rice crop samples are first analyzed using a handheld spectroradiometer. Then, multi-temporal satellite image analysis is used to determine the most suitable vegetation indices for detecting BLB. The results showed that healthy plants have the highest first derivative value of spectral reflectance of the different categories of diseased plants. Significant difference can be found at approximately 690-770 nm (red edge region) which peak or maximum of the first derivative occurs in healthy crop whereas the highest percentage of BLB showed the lowest in that region. Moreover, visible bands such as blue, green, red, and red edge 1 band show variation of correlation in the early (vegetative) to generative stage then getting high especially in early of harvesting stage than the other bands; the NIR band exhibits a low correlation from the early stage of the growing season whereas the red and red edge bands reveal the highest correlations in the later stage of harvesting. Similarly, the satellite image analysis also reveals that disease incidence gradually increases with increasing age of the plant. The vegetation indices whose formulas consist of blue, green, red, and red edge bands (NGRDI, NPCI, and PSRI) exhibit the highest correlation with BLB infestation. NPCI and PSRI indices indicate that crop stress due to BLB is detected from ripening stage of NPCI then the senescence condition is then detected 12 days later. The coefficients of determination between these indices and BLB are 0.44, 0.63, and 0.67, respectively

Keywords: BLB, handheld spectroradiometer, vegetation indices, indices change

1. Introduction

Rice is one of the most important crops for the global population. Therefore, sustainable rice farming is extremely reliant on effective pest and disease management (Zhang et al., 2002). Remote sensing of agricultural canopies can provide valuable insights into various agronomic parameters through repeated measurements that do not destroy the crop sample. Remote sensing can also be used to detect, monitor, and assess crop diseases at different spatio-temporal scales (Franke & Menz, 2007). Many previous studies have applied remote sensing to crop monitoring and disease assessment. For example, Gitelson et al. (2002) analyzed the relationship between spectral reflectance and leaf chlorophyll content, which is a measure of crop health, and reported that 520-550 nm and 695-705 nm are the most suitable spectral ranges for determining total chlorophyll content. Furthermore, the leaf area index (LAI) is the most common measure for monitoring and detecting crop diseases in a range of crops; for example, rice (Xiao et al., 2002; Qin & Zhang, 2005; Ghobadifar et al., 2016), tomato (Zhang et al, 2002), wheat (Huang & Apan, 2006), and sugar beet (Mahlein et al., 2013).

Recently, ground-based remote sensing spectral measurements have been employed as an innovative non-invasive technique for detecting vegetation status; this method provides a contiguous narrow wave-band

measure for monitoring and improved assessment of crop diseases (Adams et al., 1999; Singh et al., 2007; Das et al., 2015). For example, in order to promote the sustainable farming of rice crops, Gnyp et al. (2014) estimated above-ground biomass using hyperspectral canopy sensing to obtain an optimal measurement. Moreover, Liu et al. (2010) successfully demonstrated the feasibility of using visible and near-infrared regions in hyperspectral reflectance to detect the health condition of rice panicles (Liu et al., 2010). This technology has enormous applications on a small scale; however, it is difficult to represent entire farming regions through ground-based remote sensing.

For conducting research on a large-scale, vegetation indices represent an effective and inexpensive way to detect diseased plants, which are identified by different spectral values compared to a healthy rice crop. Several vegetation indices have been developed to extract vegetation information from satellite images; however, there is a lack of satellite-derived indexes that can directly detect vegetation changes between images with different acquisition times. Recently, the vegetation change index (Rokni & Musa, 2019) was introduced to directly detect vegetation changes between two or more different time images and has been widely developed in many fields of research, such as land use/land cover change (Huang et al., 2019), disaster management (Martinis et al., 2018), and hydrology (Zhu et al., 2011). However, evaluating seasonal patterns of vegetation indices in order to assess specific causes of damage to rice plants remains an ongoing research challenge.

More conventional methods for assessing disease-related plant damage involve visual detection by a pest observer using a sampling method; the disease area is then extrapolated based on these limited observations. However, this method has several limitations; *i.e.*, it is labor intensive, time consuming (Kobayashi, 2001; Das, 2015), and results in very approximate calculations of the area affected by the disease. Therefore, better methods are required to obtain more accurate plant damage assessments. Remote sensing technology is beneficial because it can provide detailed information on plant damage over a wide spatial area. Moreover, agricultural damage assessments are required to be precise, rapid, quantitative, and inexpensive (Hongo, 2015). Therefore, this study presents an alternative method for detecting disease-related rice crop damage that combines remote sensing with ground-based observations. Specifically, this study detects bacterial leaf blight (BLB) in a research area in Indonesia. The proposed method measures rice crop samples in different health conditions using conventional ground-based measurements as well as a spectroradiometer. The resulting reflectance values are then used to obtain the indicative values for healthy and diseased rice crop samples. Then, multi-temporal satellite images are used to determine the most suitable vegetation indices for the macroscopic detection of BLB. Moreover, the relationship between conventional ground-based observations of BLB and the spectral reflectance values is determined to analyze the disease severity in the rice crop.

2. Method

2.1 Study Area

The study was conducted in the Cihea rice irrigation area, Cianjur, West Java, Indonesia, located at 6°48' to 6°51' S and 107°15' to 107°18' E. The altitude is 200-450 m above sea level and the slope ranges from 0-40%. There are only two seasons in the study area; the dry season and the rainy season, with average annual precipitation of approximately 1000-1500 mm. The average temperature is 24.4 °C with a maximum of 30 °C from August to October and a minimum of 18 °C from July to August.

The study area predominantly produces agricultural products; specifically, it is known as the third major source of rice production in West Java Province. The Cihea rice irrigation area is divided into three parts: upstream, midstream, and downstream. Rice is grown three times a year in the upper stream area and twice a year in both the midstream and downstream areas. Test sites in this research area are typically in the midstream area due to transplanting time occurring in April to May in the dry season and November to December in the rainy season.

According to the Center of Plant Protection for Food and Horticulture of Cianjur Regency, BLB has become the most common plant disease in the last five years. Although plant loss related to BLB is minimal, the BLB infestation has become so widespread in this area that no crop is currently unaffected.

2.2 Field Data Collection

Field data was collected from the study area when the crops were ready for harvesting. Two types of data were collected; *i.e.*, the damage assessment ratio was measured by a pest observer and spectral measurements were performed by a spectroradiometer. Eight sample locations were randomly chosen to ensure a representative distribution within the midstream area; each location consisted of three different plots. The ratio of damage in each plot was observed using the conventional method by a pest observer, who sampled 10 observation points in a diagonal pattern in each plot. Each group of rice plants was assessed to determine the percentage of BLB.

Additionally, spectral data were recorded at points 1 and 10 in each plot using a MS-720 Handheld Spectroradiometer from EKO Instruments. The wavelength of the measurement was configured in the range of 350-1050 nm, the optical resolution was < 10 nm, the wavelength accuracy was less than 0.3 nm, and the field of view for the object irradiance was 45°. An incidence angle of approximately 90° was maintained at a standard distance of approximately 100 cm above the crop canopy. Each reading is the average of two replicate measurements for each object irradiance and solar irradiance value.

Conventionally, the intensity of plant disease in the research area would be expressed both quantitatively as a percentage (%), indicating the amount of plants, parts of plants, or groups of plants, and qualitatively using categories of severity; *i.e.*, mild, moderate, severe, or crop failure (Table 1).

Table 1. Category of disease severity according to the percentage of disease infestation in the research area

Category of severity	Percentage of severity
Mild	≤ 11 %
Moderate	11-25 %
Severe	25-85 %
Crop failure	> 85%

2.3 Image Collection and Pre-processing

Ten images from one planting season taken by Sentinel 2A and 2B satellites were collected from the European Space Agency (Table 2). Different types of images were collected due to variations in cloud cover over the research areas. Sentinel 2 had a total of 12 bands: Coastal Aerosol (443 nm), Water Vapor (940 nm), and SWIR Cirrus (1375 nm) with a spatial resolution of 60 m; Red Edge 1 (704 nm), Red Edge 2 (740 nm), Red Edge 3 (782 nm), and Near Infra-Red Narrow (865 nm) with a spatial resolution of 20 m; and Blue (490 nm), Green (560 nm), Red (665 nm), and Near Infra-Red (842 nm) with a spatial resolution of 10 m. For this study, the bands utilized to adjust the measurement data from the spectroradiometers were all bands with a 10-m spatial resolution and three of the bands with a 20-m spatial resolution (Red Edge 1, 2, 3). Image data were extracted using SNAP software to produce subset images of the test sites. To apply the vegetation indices and change detection, all images were geometrically registered and radiometrically normalized. Subsequently, resampling was performed to transform the images from multi-spatial resolution to a single spatial resolution.

Table 2. Satellites images used in this study, which represents a full planting season of the rice crop

Acquisition date	Satellite Images	Growth phase
May 15	Sentinel 2B	Vegetative
May 30	Sentinel 2A	Vegetative
June 9	Sentinel 2A	Reproductive
June 19	Sentinel 2A	Reproductive
June 29	Sentinel 2A	Ripening
July 9	Sentinel 2A	Ripening
July 19	Sentinel 2A	Harvesting
July 29	Sentinel 2A	Harvesting

2.4 Data Analysis

2.4.1 Reflectance Value Extraction

The spectral data collected from the handheld spectroradiometer were analyzed to obtain the reflectance values of the rice crop. The purpose of this analysis is to identify the wavelength region that can be used to distinguish diseased rice crop. By assuming a Lambertian surface (Koppal, 2014), the reflectance values were estimated as:

$$\rho = \frac{\pi I_d}{I_u \Omega} \quad (1)$$

Where, I_d is the irradiance from the object; I_u is the irradiance from the sun; and Ω is the solid view angle. The spectral reflectance derivative is widely used to eliminate background noise and atmospheric interference, identify spectral overlapping, and improve the signal-noise ratio, which in turn reduces the interference factors,

such as soil type and sample granularity, and helps define the spectral absorption properties (Fu et al., 2019). In this analysis, the first order derivative of the spectral reflectance was calculated to confirm the effect of the disease on the rice crop.

2.4.2 Vegetation Indices

Vegetation indices are used to convert the reflectance value from any source, such as spectroradiometer data or even a satellite image, into a single number in order to assess the vegetation characteristics (Singh, 2012). Multiple vegetation indices are computed in this analysis: NDVI, VCI, GNDVI, NGRDI, EVI, PSRI, and NPCI (Table 3). Plants with less than 5% BLB were considered as healthy plants due to the fact that no plants in the study area have 0% BLB. Similar to the first order derivative of reflectance data, vegetation index differencing was used to analyze vegetation changes. It is achieved by subtracting the vegetation index value of a pixel in an image taken on one date (t_1) from that in an image taken on the previous date (t_2):

$$\text{Difference} = \text{Vegetation index } t_2 - \text{Vegetation index } t_1 \quad (2)$$

Table 3. Definitions of the vegetation indices used in this study

Indices		Formula	Reference
NDVI	Normalized difference vegetation index	$(R_{\text{NIR}} - R_{\text{Red}})/(R_{\text{NIR}} + R_{\text{Red}})$	Rouse et al., 1973
GNDVI	Green normalized difference vegetation index	$(R_{\text{NIR}} - R_{\text{Green}})/(R_{\text{NIR}} + R_{\text{Green}})$	Moges et al., 2004
NGRDI	Normalized green red difference index	$(R_{\text{Green}} - R_{\text{Red}})/(R_{\text{Green}} + R_{\text{Red}})$	Tucker, 1979
VCI	Vegetation condition index	$(\text{NDVI} - \text{NDVI}_{\text{min}})/(\text{NDVI}_{\text{max}} - \text{NDVI}_{\text{min}})$	Kogan, 1995
EVI	Enhanced vegetation index	$2.5(R_{\text{NIR}} - R_{\text{Red}})/(R_{\text{NIR}} + 6R_{\text{Red}} - 7.5R_{\text{Blue}} + 1)$	Huete et al., 2002
PSRI	Plant senescence reflectance index	$(R_{\text{Red}} - R_{\text{Green}})/R_{\text{Rededge}}$	Lee et al., 2008
NPCI	Normalized pigment chlorophyll ratio index	$(R_{\text{Red}} - R_{\text{Blue}})/(R_{\text{Red}} + R_{\text{Blue}})$	Merzlyak et al., 1999

3. Results

3.1 Spectral Signature Analysis

The reflectance characteristics of rice crops according to the category of disease severity are shown in Figure 1. The significant difference between three categories were seen in green to red region (550-700 nm) and red edge to NIR region (beyond 750 nm). The plants considered healthy (< 5% BLB) have low reflectance around the green to red region and high reflectance from the red edge to NIR region. Conversely, plants with the highest percentage of BLB exhibit the opposite characteristics. The first order derivative, which shows the rate of change in the reflectance curve, is presented in Figure 2. Significant difference can be found at approximately 690-770 nm (red edge region) which peak or maximum of the first derivative occurs in healthy crop whereas the highest percentage of BLB showed the lowest in that region. Healthy plants exhibit higher first derivative values than diseased plants; therefore, disease severity appears to affect plant reflectance values. The first order derivative method could indicated healthy and diseased plants exhibit different spectral behavior (Penuelas et al., 1994; Singh et al., 2012).

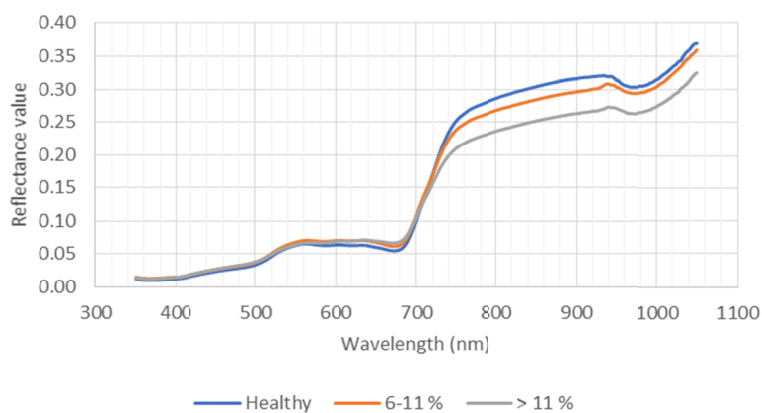


Figure 1. Reflectance signatures of rice crops according to BLB disease severity

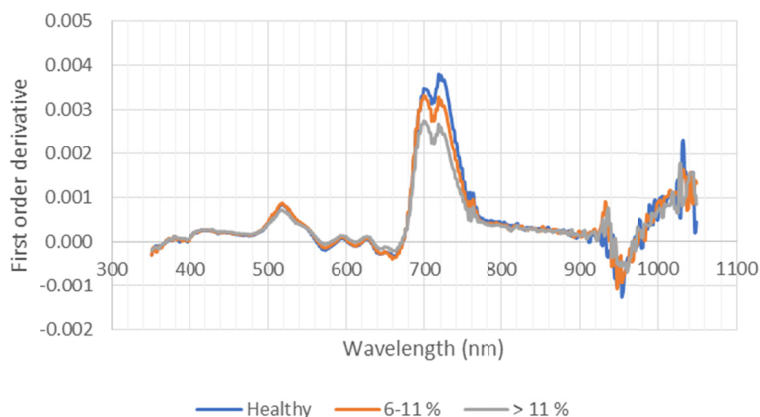


Figure 2. First order derivatives of plant spectral signatures according to BLB disease severity

The first order derivative spectral signatures of visible region; green, red, and red edge regions are shown in greater detail according to BLB severity in Figure 3. From blue region, three categorize crop show the same condition, then at green region (500-550 nm) reflectance of the diseased rice crop is decreasing than that of healthy rice; however, it then becomes higher than healthy rice in the green edge region, which likely reflects a loss of chlorophyll in the rice crop linked to yellowing and drying of the leaf caused by BLB (Figures 3A and 3B). Yellow leaves are one of the key indicators of plant stress (Adams et al., 1999). A slight change of increasing for diseased plant occurs in the red region, then the difference between healthy and diseased plants become clearer in the red edge region (Figures 3C and 3D). Land-based chlorophyll-producing crops have very strong absorption of reflectance around 700 nm (Seager et al., 2005).

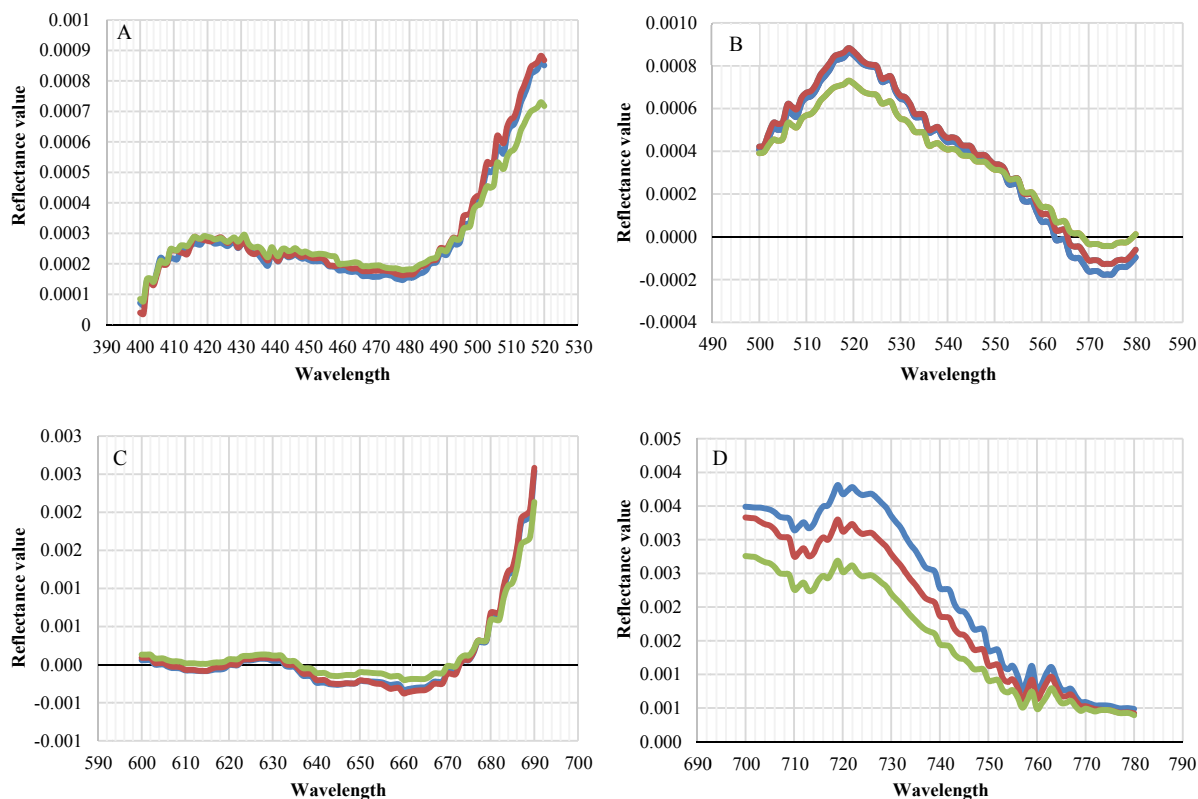


Figure 3. Detailed first order derivatives of spectral signature in (A) blue, (B) green, (C) red, and (D) red edge regions

To distinguish between healthy and diseased plants, some of the reflectance values were categorized according to wavelength using the satellites images of Sentinel-2 then compared (Table 4). According to the average spectral

value for each category, longer wavelengths are generally related to larger spectral values in both healthy and diseased plants. Furthermore, the more severely diseased the rice crop, the greater the spectral value in blue, green, and red wavelengths; however, the opposite is true for red edge and NIR wavelengths.

Table 4. Average reflectance values of rice crop according to BLB severity

Band	Wavelength	Average reflectance value			Absolute difference	
		Healthy	6-11%	> 11%	6-11%	> 11%
Blue	450-520	0.0311	0.0347	0.0352	0.00360	0.00047
Green	540-580	0.0638	0.0690	0.0655	0.00519	0.00354
Red	650-680	0.0570	0.0640	0.0680	0.00706	0.00401
Red edge	700-780	0.2223	0.2132	0.1907	0.00903	0.02256
NIR	785-900	0.3003	0.2809	0.2484	0.01948	0.03242

3.2 Satellite Image Analysis

3.2.1 Correlation between BLB, Spectral Bands, and Vegetation Indices

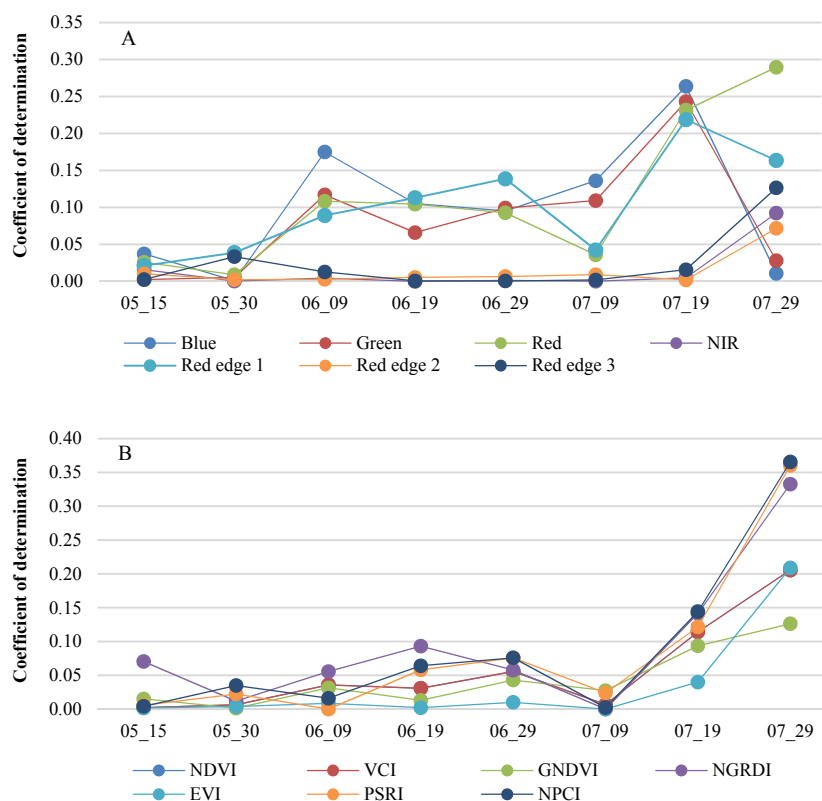


Figure 4. Correlation between BLB occurrence and (A) the reflectance value in each band and (B) vegetation indices using linear regression (coefficient of determination, R^2)

Reflectance patterns throughout the planting season reveal a large amount of information about vegetation changes at all wavelengths. Understanding these patterns is also important for interpreting the seasonal changes in vegetation indices (Hatfield & Prueger, 2010). Because multiple spectral bands and vegetation indices were used in this study, statistical analysis was conducted to highlight notable results and understand the correlation between BLB infestation and the reflectance values for each band and indices (Figure 4). It can be shown that generally, BLB has high correlation at the harvesting stage. Figure 4A shows correlation between BLB percentage and each band of Sentinel-2. Visible bands such as blue, green, red, and red edge 1 band show

variation of correlation in the early (vegetative) to generative stage then getting high especially in early of harvesting stage than the other bands; the NIR band exhibits a low correlation from the early stage of the growing season whereas the red and red edge bands reveal the highest correlations in the later stage of harvesting. Figure 4B shows clearer that high correlations are observed when the rice crop is in the ripening to harvesting stage. This indicates that disease incidence gradually increases with increasing age of the crop. It shows that NPCI, PSRI, and NGRDI have the highest correlation with BLB infestation in the rice crop. It is common knowledge that the function of the red and NIR bands are to analyze vegetation conditions; however, this study reveals that BLB infestation is more closely related to the red and red edge bands. That is, the vegetation indices with higher correlations with BLB use the red band but not the NIR band (NPCI, PSRI, and NGRDI), whereas indices that use the NIR band (NDVI, VCI, EVI, and GNDVI) exhibit lower correlations.

3.2.2 Seasonal Change in Vegetation Indices

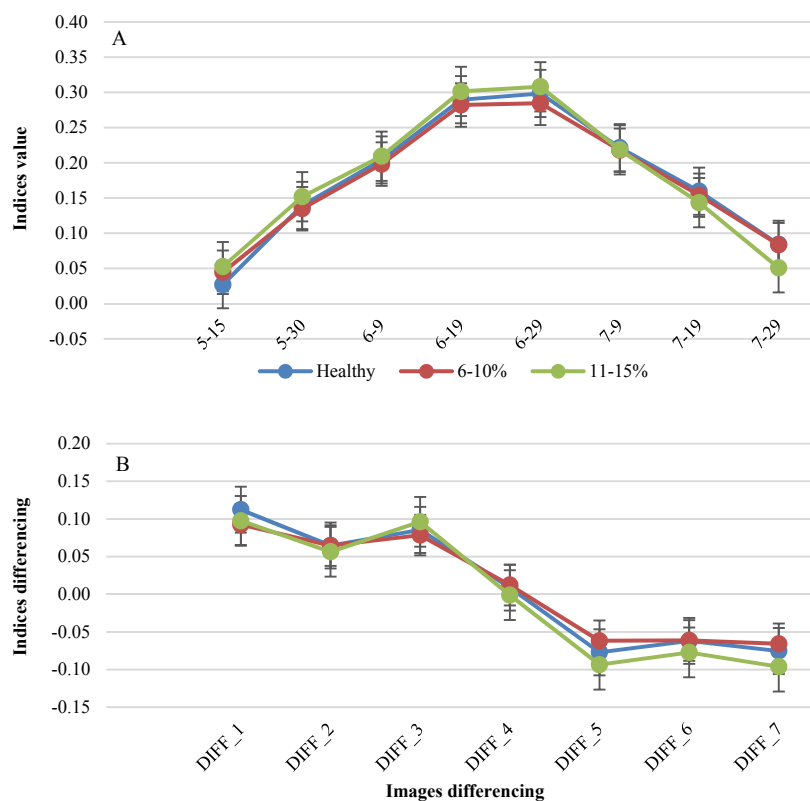


Figure 5. (A) Seasonal pattern and (B) vegetation index differencing results for the NGRDI

The seasonal change patterns for NGRDI, NPCI, and PSRI are shown in Figures 5, 6, and 7. These three indices are related to chlorophyll content on the canopy. Rice crops with high BLB severity have high NGRDI from the vegetative phase that begins to decrease in the generative phase and reaches a minimum in the harvesting stage (Figure 5A). Additionally, Figure 5B reflects that the rice crop started to become yellow at the transition between the vegetative stage and the generative stage (Diff_4). The reason for this yellowness is unclear because the indices do not indicate the condition of the crop itself.

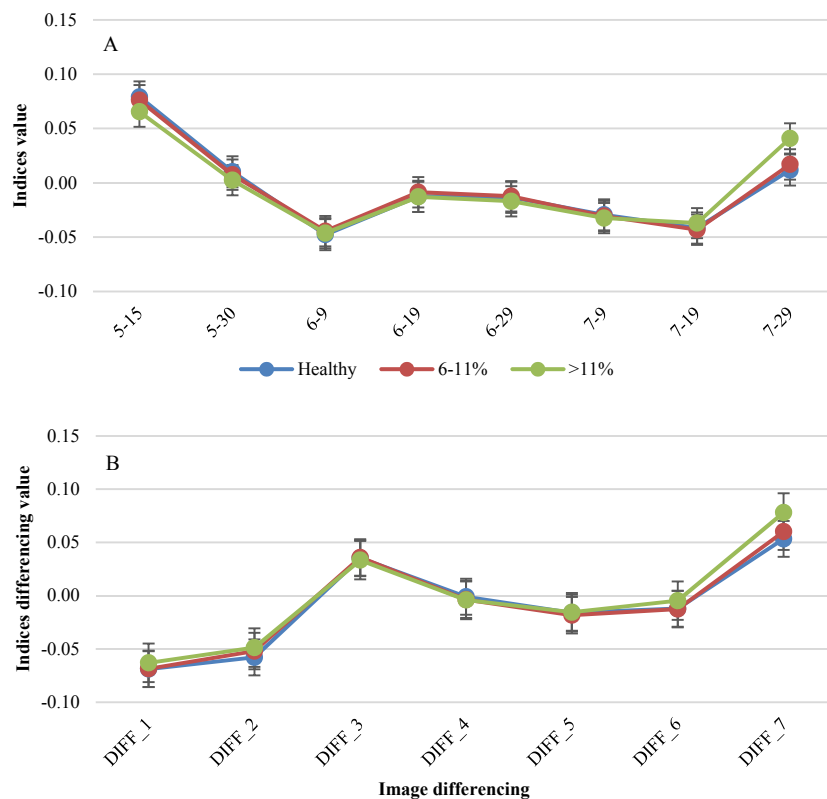


Figure 6. (A) Seasonal pattern and (B) vegetation index differencing results for the PSRI

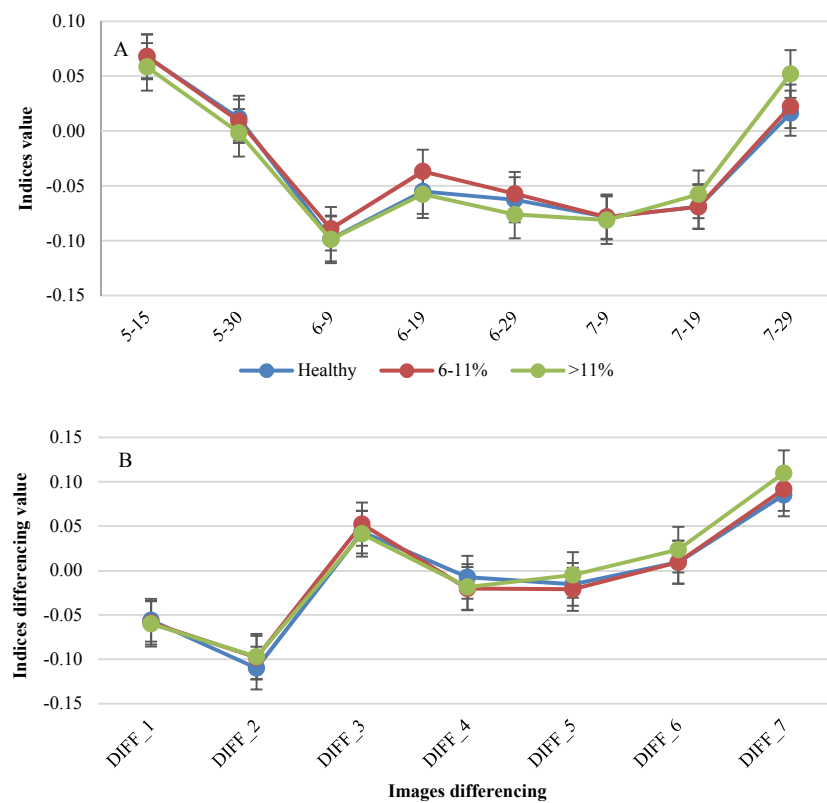


Figure 7. (A) Seasonal pattern and (B) vegetation index differencing results for the NPCI

PSRI and NPCI show similar characteristics to each other. PSRI and NPCI are high in the early stages of the rice season then start to decrease and become high again in the later stages or when the crop is ready to be harvested (Figures 6A and 7A). NPCI shows greater variability than PSRI from the later phase of the vegetative stage into the early generative stage. The PSRI values indicate decrease conditions of rice crop at harvesting stage (from July 19), whereas NPCI values suggest that the crop condition is decreasing from the ripening stage (from June 29). The differencing results of both indices also show some similarities (Figures 6B and 7B) that the change in vegetation conditions begins from the generative phase. According to PSRI, the stress level of the rice crop increases from Diff_5 (difference between July 9 and June 29). Conversely, according to NPCI, the stress level starts to increase earlier, in Diff_4 (difference between June 29 and June 19) which indicates that the effects of BLB are notable at this time, and senescence is detected 12 days later.

4. Discussion

Using first order derivative method can show that the significance difference of healthy and diseased crop were in green and red edge region. For vegetation analysis, green region is closely related to the greenness whereas BLB affection caused plant becomes yellowing and dry. Red edge also important to because the steep change of reflectance occurs in this region. This region's position also categorized as main inflexion point of the red-NIR slope and can be used to estimate the chlorophyll content (Clevers et al., 2010). For BLB affection, it attacks the leaf tissue and destroys the chlorophyll so that the channels of nutrient and energy distribution become obstructed.

Green and red band were used in NGRDI's formula, but the result did not show significance difference. NGRDI is commonly used to estimate the vegetation fraction and is considered as a phenology indicator for biomass estimation (Wan et al., 2018). Although statistically this indices show high correlation with BLB occurrence but the actual relationship were not compatible. PSRI and NPCI show different result compare to NGRDI. The similar NPCI and PSRI patterns can be explained by the fact that these indices focus on the chlorophyll ratio and plant senescence. These show a slight change for diseased plants after the reproductive stage then increase as the crop matures and the leaf color begins to change. NPCI is more sensitive to changes in chlorophyll in the later stages of rice growth due to the decreasing demand for nutrients (Hatfield & Prueger, 2010). Conversely, PSRI is designed to maximize the sensitivity of the ratio of bulk carotenoids, such as alpha-carotene and beta-carotene, to chlorophyll. An increase of PSRI indicates increased stress in the canopy, the onset of canopy senescence, and plant ripening (Das et al., 2015). Higher values indicate a greater possibility that the rice crop is under stress conditions that could lead to nutrient deficiency.

Statistical analysis using linear regression to see the correlation and significance variable were used in this study (Table 5). P-value for each indices were showed based on the acquisition date. This result supports the satellite image analysis that BLB occurrence mostly can be seen in the later phase (harvesting stage). PSRI is an effective indices that has the highest correlation and significance to BLB occurrence with 0.013 ($\alpha = 0.05$) as well as NPCI with significance value 0.031. Coefficient of determination for NGRDI, NPCI, and PSRI are 0.44, 0.63 and 0.67 respectively. This shows that Sentinel-2 with 10-m spatial resolution is useful to detect BLB disease in rice crop. This study could be improved by incorporating external factors such as altitude, rainfall, and sample chlorophyll contents, as well as satellite images with a better spectral, spatial, and temporal resolution. Limitation of this analysis is that it cannot detect rice crop condition in the vegetative phase, especially after transplanting, due to rice crop coverage is too small compare to the water coverage.

Table 5. Linier regression analysis for NGRDI, NPCI and PSRI

Acquisition Date	NGRDI	NPCI	PSRI
5/15	0.969	0.335	0.866
5/30	0.612	0.382	0.625
6/9	0.815	0.492	0.166
6/19	0.709	0.829	0.769
6/29	0.675	0.484	0.394
7/9	0.600	0.148	0.194
7/19	0.946	0.804	0.475
7/29	0.120	0.008*	0.004*
Significance-F	0.272	0.0031*	0.013*
Multiple R	0.654	0.785	0.817
R ²	0.438	0.626	0.668

Acknowledgements

This research is supported by the Science and Technology Research Partnership for Sustainable Development (SATREPS); a collaborative project between the Japan Science Technology Agency (JST) and the Japan International Corporation Agency (JICA). Mr. Dede Ruswana is also acknowledged as the pest observer who conducted the assessments of the BLB damage ratio.

References

- Adams, M. L., Philpot, W. D., & Novell, W. A. (1999). Yellowness index: an application of spectral second derivative to estimates chlorosis of leaves in stressed vegetation. *Int. J. Remote Sens.* 20 (18):3633-3675. <https://doi.org/10.1080/014311699211264>
- Clevers, J. G. P. W., De Jong, S. M., Epema, G. F., Van Der Meer, F. D., Bakker, W. H., Skidmore, A. K., & Scholte, K. H. (2010). Derivation of the red edge index using MERIS standard band setting. *Int. J. Remote Sensing*, 2(16), 3169-3184. <https://doi.org/10.1080/01431160110104647>
- Das, P. K., Laxman, B., Rao, S. V. C. K., Seshasai, M. V. R., & Dadhwal, V. K. (2015). Monitoring of bacterial leaf blight in rice using ground-based hyperspectral and LISS IV satellites data in Kurnool, Andhra Pradesh, India. *Int. J. of Pest Man.*, 61(4), 359-368. <https://doi.org/10.1080/09670874.2015.1072652>
- Franke, J., & Menz, G. (2007). Multi-spectral wheat disease detection by multi-spectral remote sensing. *Precis. Agric.*, 8, 161-172. <https://doi.org/10.1007/s11119-007-9036-y>
- Fu, C. B., Xiong, H. G., & Tian, A. H. (2019). Study on the effect of fractional derivative on the hyperspectral data of soil organic matter content in arid region. *J. of Spectros.*, 11. <https://doi.org/10.1155/2019/7159317>
- Ghobadifar, F., Wayayok, A., Mansor, S., & Shafri, H. Z. (2016). Detection of BPH (brown planthopper) sheath blight in rice farming using multispectral remote sensing. *Geomatics, Natural Haz and Risk*, 7(1), 237-247. <https://doi.org/10.1080/19475705.2014.885468>
- Gitelson, A. A., Kaufman, Y. J., Stark, R., & Rundquist, D. (2002). Novel algorithms for remote sensing estimation of vegetation fraction. *Remote Sens. Environ.*, 80, 76-87. <https://doi.org/10.1078/0176-1617-00887>
- Gnyp, M. L., Miao, Y., Yuan, F., Ustin, S. L., Yu, K., Yao, Y., ... Bareth, G. (2014). Hyperspectral canopy sensing of paddy rice aboveground biomass at different growth stage. *Field Crop Res.*, 155, 42-55. <https://doi.org/10.1016/j.fcr.2013.09.023>
- Hatfield, J. L., & Prueger, J. H. (2010). Value of using vegetative indices to quantify agricultural crop characteristics at different growth stage under varying management practices. *Remote Sens.*, 2, 562-578. <https://doi.org/10.3390/rs2020562>
- Hongo, C., Tsuzawa, T., Tokui, K., & Tamura, E. (2015). Development of damage assessment method of rice crop for agricultural insurance using satellite data. *Journal of Agricultural Science*, 7(12), 59-71. <https://doi.org/10.5539/jas.v7n12p59>
- Huang, C., Huang, X., Peng, C., Zhou, Z., Teng, M., & Wang, P. (2019). Land use/cover change in the Three gorges Reservoir area, China: reconciling the land use conflicts between development and protection. *Catena*, 175, 388-399. <https://doi.org/10.1016/j.catena.2019.01.002>

- Huang, J. F., & Apan, A. (2006). Detection of sclerotinia rot disease in celery using hyperspectral data and partial least squares regression. *J. Spat. Sci.*, *52*, 129-142. <https://doi.org/10.1080/14498596.2006.9635087>
- Huete, A., Didan, K., Miura, T., Rodriguez, E. P., Gao, X., & Ferreira, L. G. (2002). Overview of the radiometric and biophysical performance of the MODIS vegetation indices. *Remote Sens. Environ.*, *83*, 195-213. [https://doi.org/10.1016/S0034-4257\(02\)00096-2](https://doi.org/10.1016/S0034-4257(02)00096-2)
- Kobayashi, T., Kanda, E., Kitada, K., Ishiguro, K., & Torigoe, Y. (2001). Detection of rice panicle blast of multispectral radiometer and the potential of using airborne multispectral scanners. *Phytopathology*, *91*:316-323. <https://doi.org/10.1094/PHYTO.2001.91.3.316>
- Kogan, F. N. (1995). Droughts of the late 1980s in the United States as derived from NOAA polar-orbiting satellite data. *Bull. Am. Meteorol. Soc.*, *76*, 655-668. [https://doi.org/10.1175/1520-0477\(1995\)076%3C0655:DOTLIT%3E2.0.CO;2](https://doi.org/10.1175/1520-0477(1995)076%3C0655:DOTLIT%3E2.0.CO;2)
- Koppal, S. J. (2014). Lambertian reflectance. In K. Ikeuchi (Eds.), *Computer Vision*. Springer, Boston, MA. https://doi.org/10.1007/978-0-387-31439-6_534
- Lee, Y., Yang, C., Chang, K., & Shen, Y. A. (2008). A simple spectral index using reflectance of 735 nm to assess nitrogen status of rice canopy. *Agron. J.*, *100*, 202-212. <https://doi.org/10.2134/agronj2007.0018>
- Liu, Z., Shi, J., Zhang, L., & Huang, J. (2010). Discrimination of rice panicles by hyperspectral reflectance data based on principal component analysis and support vector classification. *Journal of Zhenjiang Univ., Science B*, *11*(1), 71-78. <https://doi.org/10.1631/jzus.B0900193>
- Mahlein, A. K., Steiner, U., Hihnutter, C., Dehne, H. W., & Oerke, E. C. (2013). Hyperspectral imaging for small-scale analysis of symptoms caused by different sugar beet diseases. *Plant Methods*, *8*, 1-13. <https://doi.org/10.1016/j.rse.2012.09.019>
- Martinis, S., Plank, S., & Cwik, K. (2018). The use of Sentinel-1 time series data to improve flood monitoring in arid areas. *Remote Sens.*, *10*, 583. <https://doi.org/10.3390/rs10040583>
- Merzlyak, M. N., Gitelson, A. A., Chivkunova, O. B., & Rakitin, V. Y. (1999). Non-destructive optical detection of leaf senescence and fruit ripening. *Physiol. Plant*, *106*, 135-14. <https://doi.org/10.1034/j.1399-3054.1999.106119.x>
- Moges, S. M., Raun, W. R., Mullen, R. W., Freeman, K. W., Johnson, G. V., & Solie, J. B. (2004). Evaluation of green, red and near infrared bands for predicting winter wheat biomass, nitrogen uptake and final grain yield. *J. Plant Nutr.*, *27*(8), 1431-1441. <https://doi.org/10.1081/PLN-200025858>
- Penuelas, J., Gamon, J. A., Fredeen, A. L., Merino, J., & Field, C. B. (1994). Reflectance indices associated with physiological change in nitrogen and water-limited sunflower leaves. *Remote Sens. Environ.*, *48*, 135-146. [https://doi.org/10.1016/0034-4257\(94\)90136-8](https://doi.org/10.1016/0034-4257(94)90136-8)
- Qin, Z., & Zhang, M. (2005). Detection of rice sheath blight for in-season disease management using multispectral remote sensing. *Int. J. Appl. Earth Obs. Geoinf.*, *7*, 115-128. <https://doi.org/10.1016/j.jag.2005.03.004>
- Rokni, K., & Musa, T. A. (2019). Normalized difference vegetation change index: A technique for detecting vegetation changes using Landsat imagery. *Catena*, *178*, 56-63. <https://doi.org/10.1016/j.catena.2019.03.007>
- Rouse, J. W., Haas, R. H., Schell, J. A., & Deering, D. W. (1973). Monitoring vegetation system in a great plains with ERTS. *Proceeding of 3rd Earth Resources Technology Satellite-1 Symposium* (pp. 48-62). Maryland, United States of America: National Aeronautics and Space Administration.
- Seager, S., Turner, E. L., Schafer, J., & Ford, E. B. (2005). Vegetation's red edge: A possible spectroscopic biosignature of extraterrestrial plants. *Astrobiology*, *5*(3), 372-390. <https://doi.org/10.1089/ast.2005.5.372>
- Singh, B., Singh, M., Singh, G., Suri, K., Pannu, P. P. S., & Bal, S. K. (2012). Hyperspectral data for the detection of rice bacterial leaf blight (BLB) disease. *Proceeding of 3rd National Conference on Agro-Informatics and Precision Agriculture* (pp. 177-182). Hyderabad, India: Indian Society of Agricultural Information Technology (INSAIT).
- Singh, D., Sao, R., & Singh, K. P. (2007). A remote sensing assessment of pest infestation on sorghum. *Adv. Space. Res.*, *39*(1), 155-163. <https://doi.org/10.1016/j.asr.2006.02.025>

- Tucker, C. J. (1979). Red and photographic infrared linear combination for monitoring vegetation. *Remote Sens. Environ.*, 8, 127-150. [https://doi.org/10.1016/0034-4257\(79\)90013-0](https://doi.org/10.1016/0034-4257(79)90013-0)
- Wan, L., Li, Y., Cen., H., Zhu, J., Yin, W., Wu, W., ... He, Y. (2018). Combining UAV-based vegetation indices and image classification to estimates flower number in oilseed rape. *Remote Sens.*, 10, 1484. <https://doi.org/10.3390/rs10091484>
- Xiao, X., He, L., Salas, W, Li, C., Moore, B., Zhao, R., Froking, S., & Boles, S. (2002). Quantitative relationships between field-measured leaf area index and vegetation index derived from vegetation images for paddy rice fields. *Int. J. Remote Sens.*, 23(18), 3595-3604. <https://doi.org/10.1080/01431160110115199>
- Zhang, M., Liu, X., & O'Neill, M. (2002). Spectral discrimination of phytophthora infestans infection on tomatoes based on principle component and cluster analysis. *Int. J. Rem. Sens.*, 23(6), 1095-1107. <https://doi.org/10.1080/01431160110106078>
- Zhu, X., Cao, J., & Dai, Y. (2011). A decision tree model for meteorological disaster grade evaluation of flood. *Proceeding of 4th International Joint Conference on computational Science and Optimization* (pp. 916-919). Yunan, China: Institute of Electrical and Electronics Engineers (IEEE). <https://doi.org/10.1109/CSO.2011.26>

Copyrights

Copyright for this article is retained by the author(s), with first publication rights granted to the journal.

This is an open-access article distributed under the terms and conditions of the Creative Commons Attribution license (<http://creativecommons.org/licenses/by/4.0/>).